

# Naturally weathered feldspar surfaces in the Navajo Sandstone aquifer, Black Mesa, Arizona: Electron microscopic characterization

Chen Zhu <sup>a,\*</sup>, David R. Veblen <sup>b</sup>, Alex E. Blum <sup>c</sup>, Stephen J. Chipera <sup>d</sup>

<sup>a</sup> Department of Geological Sciences, Indiana University, Bloomington, IN 47405, USA

<sup>b</sup> Department of Earth and Planetary Science, Johns Hopkins University, Baltimore, MD 21218, USA

<sup>c</sup> US Geological Survey, 3215 Marine Street, Boulder, CO 80308, USA

<sup>d</sup> Earth and Environmental Sciences, Los Alamos National Laboratory, Los Alamos, NM 87545, USA

Received 17 February 2006; accepted in revised form 14 July 2006

## Abstract

Naturally weathered feldspar surfaces in the Jurassic Navajo Sandstone at Black Mesa, Arizona, was characterized with high-resolution transmission and analytical electron microscope (HRTEM-AEM) and field emission gun scanning electron microscope (FEG-SEM). Here, we report the first HRTEM observation of a 10-nm thick amorphous layer on naturally weathered K-feldspar in currently slightly alkaline groundwater. The amorphous layer is probably deficient in K and enriched in Si. In addition to the amorphous layer, the feldspar surfaces are also partially coated with tightly adhered kaolin platelets. Outside of the kaolin coatings, feldspar grains are covered with a continuous 3–5  $\mu\text{m}$  thick layer of authigenic smectite, which also coats quartz and other sediment grains. Authigenic K-feldspar overgrowth and etch pits were also found on feldspar grains. These characteristics of the aged feldspar surfaces accentuate the differences in reactivity between the freshly ground feldspar powders used in laboratory experiments and feldspar grains in natural systems, and may partially contribute to the commonly observed apparent laboratory-field dissolution rate discrepancy. At Black Mesa, feldspars in the Navajo Sandstone are dissolving at  $\sim 10^5$  times slower than laboratory rate at comparable temperature and pH under far from equilibrium condition. The tightly adhered kaolin platelets reduce the feldspar reactive surface area, and the authigenic K-feldspar overgrowth reduces the feldspar reactivity. However, the continuous smectite coating layer does not appear to constitute a diffusion barrier. The exact role of the amorphous layer on feldspar dissolution kinetics depends on the origin of the layer (leached layer versus re-precipitated silica), which is uncertain at present. However, the nanometer thin layer can be detected only with HRTEM, and thus our study raises the possibility of its wide occurrence in geological systems. Rate laws and proposed mechanisms should consider the possibility of this amorphous layer on feldspar surface.

© 2006 Elsevier Inc. All rights reserved.

## 1. Introduction

Several mechanisms have been proposed to explain the widely observed two to five orders of magnitude apparent discrepancy between field and laboratory measured feldspar dissolution rates at similar temperatures and pH (Paces, 1983; Velbel, 1985; Velbel, 1990; Brantley, 1992; Blum and Stillings, 1995; Drever and Clow, 1995; White et al., 2001; White and Brantley, 2003). One set of possible mech-

anisms involves characteristics of the unsaturated zone, such as the complexity of unsaturated hydrology which may lead to incomplete wetting of mineral surface and/or a lack of effective connection between pore waters, the effects of wetting and drying cycles, and biologic effects of both macrobiotic and microbiotic communities. Recently, Zhu et al. (2004) and Zhu (2005) derived *in situ* feldspar dissolution rates in the saturated Navajo Sandstone of Black Mesa, a regional aquifer. They found plagioclase and K-feldspar dissolution rates are even slower than those in near surface systems. This suggests that the retardation of feldspar reaction rates is not dominated by unique characteristics confined in the unsaturated zone only. The slow

\* Corresponding author. Fax: +1 812 856 2223.

E-mail address: [chenzhu@indiana.edu](mailto:chenzhu@indiana.edu) (C. Zhu).

rate of silicate reactions has also been shown in several other regional aquifers (Zhu and Blum, 2005).

Another set of mechanisms for the retardation of feldspar dissolution rates is based on the hypothesis that the surface characteristics of “aged” feldspar surfaces may be significantly different from those of freshly ground feldspar powders used in most laboratory dissolution experiments. The potential importance of aged mineral surface in natural systems was recently supported by White and Brantley (2003), who found an inverse relationship between natural feldspar dissolution rates and the logarithm of ages of weathering systems. White and Brantley (2003) emphasized the different silicate reactivity resulting from surface aging and surface coating that represent the intrinsic properties of the reactants. While a vast literature has been accumulated on the topic of silicate reaction kinetics, only scant

data are available on the surface characteristics of silicates from natural systems. As a result, the term “feldspar–water interface” is widely used but its meaning remains to be vague. Fig. 1 depicts a variety of configurations or hypotheses of the interfaces in the literature.

In this work, we examined the surface characteristics of feldspars in the Navajo aquifer at Black Mesa, a long lived natural weathering system. The Navajo Sandstone was deposited ~200 million years ago. The feldspars in the sandstone have undergone many stages of reactions and are thus “aged” significantly as compared to fresh ground feldspar powders in the laboratory experiments. Currently, these feldspars have also been reacting with groundwater for the past a few millions of years (Zhu, 2005). Therefore, these feldspar samples provide an opportunity to examine their surface characteristics, which cannot be replicated in

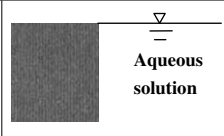
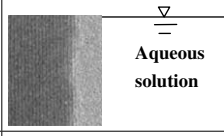
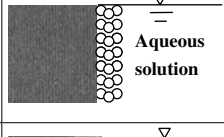
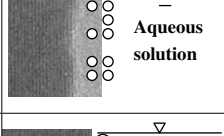
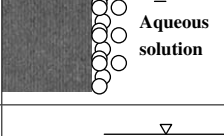
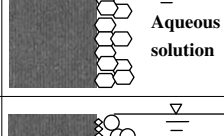
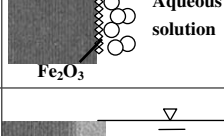
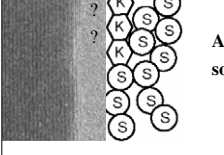
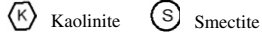
1		Pristine feldspar in contact with water, and surface reactions controls the dissolution kinetics (Lagache et al., 1961).
2		There is an alkali and Al deficient leached layer, which is in direct contact with water (Paces, 1973).
3		Crystalline feldspars have sharp boundary with re-precipitated amorphous silica (Hellmann et al., 2003). Leached layer is an artifact of analytical techniques.
4		Collapsed, re-polymerized, porous and re-structured leached layer (Casey et al., 1989).
5		Amorphous precipitates on (crystalline) feldspar surface (Correns and von Engelhardt, 1938).
6		Crystalline secondary mineral precipitates on (crystalline) feldspar surface (Helgeson, 1971).
7		Iron oxide binding negatively charged clayey coating and negatively charged feldspar surface.
8		At Black Mesa, 10 nm thick amorphous layer covered by a discontinuous kaolinite layer, and in turn covered by a smectite layer. 

Fig. 1. Various hypotheses of the feldspar–water interfaces.

laboratory aging experiments. Here, we report results using field emission gun scanning electron microscopy (FEG-SEM), associated energy dispersive X-ray spectroscopy (EDS), and high resolution transmission electron microscopy (HRTEM) and analytical electron microscopy (AEM) to analyze the naturally weathered feldspar surfaces. The geochemistry of groundwater that has been reacting with these feldspars and the *in situ* feldspar dissolution rates derived from the solute fluxes with the inverse mass balance modeling method was described in Zhu (2005).

## 2. Geology, hydrology, and geochemistry settings

The Early Jurassic (190–180 ma) Navajo Sandstone in Arizona was part of the largest ancient dune field in North America, covering an area the size of the present-day Sahara desert (Blakey et al., 1988). Various theories for sediment provenance have been suggested, ranging from uplifted central Montana area, reworked older aeolian units, or the Appalachians through a continental scale fluvial transport system (Peterson, 1988; Rahl et al., 2003).

The Navajo Sandstone has a maximum thickness of 670 m. The Late Cretaceous–Early Tertiary Laramide Orogeny folded and thrust the Navajo Sandstone to different deformation and burial depths (Libarkin and Chase, 2003; Sahagian et al., 2003). In the Wyoming overthrust belt, illite formation occurred around 145–94 ma at a temperature of 80–125 °C, heated by basinal fluid flow (Aronson and Buntner, 1983; Buntner and Nigrini, 1994). The Black Mesa area experienced only shallow burial, with post-Laramide erosion estimated at only 500–1000 m (Pederson et al., 2002).

In the Black Mesa area, the Navajo Sandstone has a relatively uniform lithology composed of medium- to fine-grained quartz sands (Harshbarger et al., 1957; Dulaney, 1989). The Navajo Sandstone is generally sub-horizontal in the Black Mesa area (Cooley et al., 1969), and the current burial depth is ~1000–1500 m. As shown below, almost no illite was found in the Navajo Sandstone at Black Mesa, and quartz overgrowths are thin. The Navajo Sandstone forms the most productive unit of the Navajo or N-aquifer in the Black Mesa region (Cooley et al., 1969; Eychaner, 1983; Brown and Eychaner, 1988; Zhu et al., 1998; Zhu, 2000). Groundwater pH typically ranges from 7.5 to 8.0, with maximum values of almost 9.5. Groundwater temperatures range from 15 to 35 °C due to depth and thermal gradient effects. See Cooley et al. (1969), Eychaner (1983), Zhu (2000, 2005), Zhu et al. (1998, 2003), and references therein for more on the background groundwater geochemistry and hydrogeology.

## 3. Sampling and experimental methods

### 3.1. Sampling and size fractionation

Drill cuttings and drill cores of the Navajo Sandstone were collected in the area (Fig. 2). To supplement the

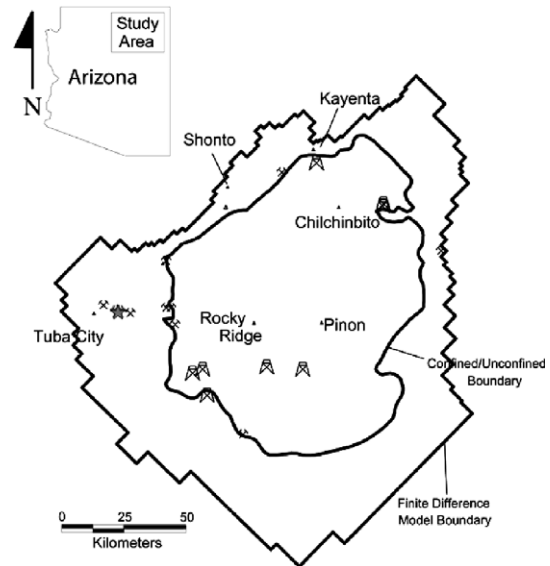


Fig. 2. Locations of Navajo Sandstone samples at Black Mesa. Hammers indicate outcrops; well symbols indicate drill cuttings from oil and gas exploration wells; stars (five overlapped) denote drill cores. Triangles are locations of towns; and the town names are besides the triangles. The “finite difference model boundary” and “confined/unconfined boundary” refer to the two-dimensional finite difference groundwater flow model discussed in Zhu et al. (1998). Sample locations were overlain on the groundwater model and town locations with a Geographic Information System software.

drill core and drill cutting samples, outcrop samples were also obtained (Fig. 2). The sediment grains in the Navajo Sandstone are coated with clay minerals (see below). A Fisher FS 20 Ultrasonic cleaner was used to remove the coatings on the Navajo Sandstone grains. The samples were sonicated for 10 min. The supernatant (SN) was decanted into 200 ml centrifuge bottles and capped. The beaker was then refilled with deionized water and sonicated for another 10 min. The bottles containing the supernatants were centrifuged in a Beckman CS-6KR centrifuge at 3600 rpm for 60 min. All supernatants were clear after centrifugation. The SN was decanted, and the clay fraction in the bottles was vacuum filtered with a Millipore type VCTP 0.1 μm filter and collected for analysis.

### 3.2. X-ray diffraction

Both bulk samples and clay fractions were analyzed by X-ray diffraction (XRD) on a Siemens D-500 diffractometer with incident- and diffracted-beam Soller slits, a KeveX PSI solid-state detector, and CuKα radiation. The samples were step-scanned from 2° to 60° 2θ with a counting time of 2 s per step. Oriented mounts were prepared on an off-axis quartz plate, and X-ray data were collected either in low relative-humidity air or after ethylene glycol solvation to distinguish expandable clays. For semi-quantitative estimate of mineral abundances, Al<sub>2</sub>O<sub>3</sub> was used as an internal standard.

### 3.3. Electron microscopy and electron microprobe analysis

Scanning electron microscopy (SEM) was conducted with a Philips XL 30-field emission gun (FEG) SEM and a RJ Lee instruments personal SEM. The FEG-SEM has secondary and back scattered electron detectors for imaging, as well as an energy dispersive X-ray spectrometer with an EDAX ultrathin window CDU LEAP detector capable of analyzing light elements down to carbon. Sandstone cores were made into double-sided, polished petrographic thin-sections. The drill cutting samples were mixed with epoxy, secured into 1-in. phenol rings and gently polished to a smooth, flat surface. For grain mounts, sand grains were sprinkled onto double-sided tape. A large number of samples were examined using a RJ Lee instruments personal SEM. Samples were coated with a layer of palladium or carbon before SEM analysis. The compositions of feldspars were determined by wavelength dispersive X-ray spectroscopy using a CAMECA SX50 electron microprobe.

TEM observations were performed using a Philips CM300FEG microscope operated at 295 kV and a JEOL 2010 microscope operated at 200 kV. X-Ray microanalyses were performed using a Philips EM 420 microscope equipped with an Oxford Si (Li) energy-dispersive X-ray system (EDS) and analytical software desk top spectrum analyzer (DTSA) from the National Institute of Standards and Technology. Data reduction were carried out using the standard Cliff–Lorimer method implemented in the DTSA.

Two TEM sample preparation methods were used, crushing and ion milling. In the first method, samples were ground in an agate mortar, suspended in ethanol, and then dropped on holey carbon film supported by a standard Cu TEM grid and air-dried. In the second method, specimens were prepared by cutting from petrographic thin sections and mounted onto single-hole Cu grids. Cu grids were mounted on the focus area, and the sample was further thinned to ~100 nm, using an ion beam. Finally, a very thin carbon film was coated onto the ion milled samples.

## 4. Results and discussion

### 4.1. Mineralogical compositions of Navajo Sandstone at Black Mesa

XRD analysis of the bulk Navajo Sandstone at Black Mesa shows ~90% wt quartz, with minor amounts of

K-feldspar and smectite, and trace amounts of kaolinite, illite/mica, and hematite (Table 1). The method of semi-quantitative data deduction used in this study was described previously (Chipera and Bish, 2002). Although the aeolian Navajo Sandstone is as lithologically homogeneous as it can be in nature, spatial heterogeneities in mineral abundances are, nevertheless, expected in our study area. Net (2003) found a much higher percentage of feldspars in samples collected in Utah and Wyoming, but the mineralogical assemblages in her samples are similar to ours. Beitler et al. (2005) conducted both point counting and whole-rock chemical analysis, and found about 4% feldspars in their samples.

Our XRD results are consistent with our optical microscopy, electron microprobe, and SEM observations, which also identified calcite, plagioclase, Fe–Ti oxides, apatite, and barite in the Navajo Sandstone samples. Twenty-five electron microprobe analyses show that the K-feldspars have less than 5% Na/(Na + K), with little Ca, and with ~0.1 wt% BaO. These observations are consistent with previous petrographic studies and XRD results at Black Mesa (Harshbarger et al., 1957; Dulaney, 1989).

XRD analysis of oriented and glycolated mounts of the clay suspension revealed smectites as being dominant in the clay fraction (>95%), with small amounts of kaolin (Fig. 3). A small 10 Å peak is present in the XRD patterns, which is either a detrital mica or illite interstratified with smectite.

### 4.2. Clay coatings

All observed feldspar grains are coated with a continuous layer of clayey materials (Figs. 4 and 5). The clay coating covers quartz and K-feldspar overgrowth. The thickness of the coating layer ranges from 1 to 5 µm, but varies from grain to grain and from sample to sample.

Fig. 4 shows the coating layer on a feldspar surface in a drill cutting sample. The SEM-EDS spectrum detected Si, Al, Mg, Fe, and Ca, suggesting a composition close to smectite (see below), which is consistent with XRD results. Feldspar “remnants” of variable sizes are embedded in the coating layer, and the clayey materials wrap around these remnants. The coating materials also have developed in crevices and fissures within the feldspar grain interiors and along cleavages, forming weathering fronts (Fig. 4d–f). These textural relations suggest that the smectite clays in the grain coatings are weathering products formed *in situ*, and are not of detrital origin. Smectite coatings

Table 1  
Semi-quantitative estimates of mineral abundances from XRD patterns (wt %) in the Navajo Sandstone at Black Mesa

Sample	Quartz	Smectite	Kaolinite	K-Feldspar	Mica	Hematite	Total
MSE-1, 114.5	80	5	<0.4	5	<0.3	<0.1	91
MSE-1(2), 136.5–137	92	4	<0.3	4	<0.4	—	101
MSE-2, 148–148.5	92	3	<0.1	4	<0.2	—	100
MSE-4, 88.3–85.8	93	4	<0.1	2	<0.3	—	98
Average	89%	4	<0.2%	4%	<0.3%		



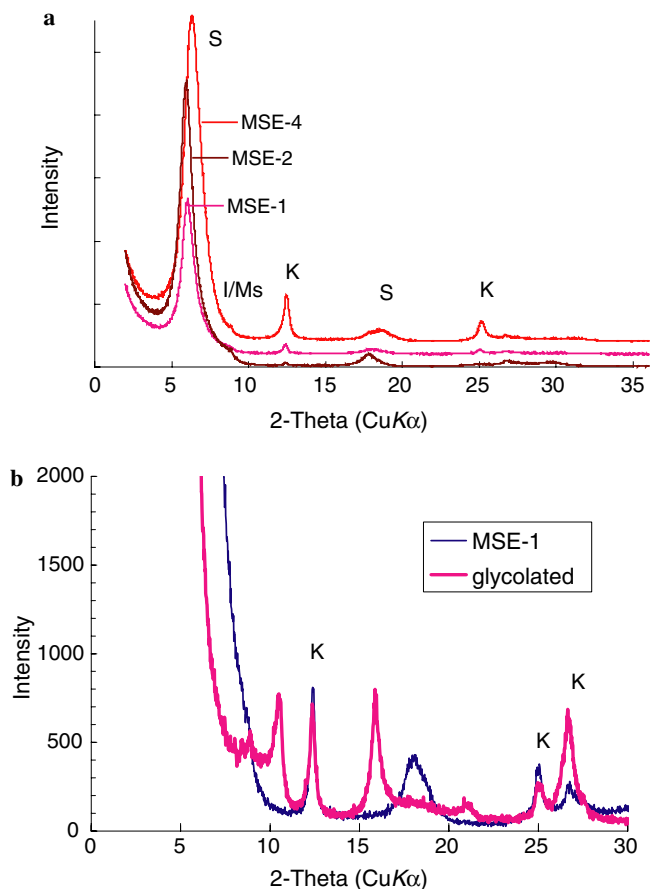


Fig. 3. X-ray diffraction patterns of oriented clay mounts on an off-axis quartz plate. (a) Patterns are scaled to produce comparable intensities for the smectite 001 peak (S); and (b) comparison with glycol-solvated sample for MSE-1. “K” stands for kaolinite, “I” illite, “Ms” muscovite.

do not occur only on feldspar grains, but also on quartz, and Fe–Ti oxide grains (Fig. 4b).

Grain-mounted SEM samples clearly show the textural relationships of these feldspar coatings (Fig. 5). Feldspars are first covered with a layer of kaolin mineral, probably kaolinite, and then a layer of smectite (Fig. 5a and b). The kaolinite is euhedral to semi-euhedral hexagonal platelets, with the edge of 100–500 nm in length. These platelets are well oriented (Fig. 5c). Chemical analyses showed only Al, Si, O EDS spectra (Fig. 5d). The basal plane always faces the feldspar surface. On a single feldspar grain, kaolinite only appears on part of feldspar surfaces and never forms a continuous cover. Kaolinite also appears in the etch-pit or cavities of K-feldspar. See more on kaolinite in samples when the smectite was ultrasonically removed in Section 4.3. Despite our deliberate efforts, we never observed kaolin on quartz grains.

The smectite has corn flake shapes (Fig. 5e and f). These corn flake smectite coatings also appear on quartz grains (Fig. 5g and h). No lath shaped clay particles were observed. Corn flake shaped smectite typically represents those formed at low-temperatures. With increasing temperature and deeper burial, smectite would transform to illite,

and clay particles would have more lath shaped particles (Moore and Reynolds, 1997). The absence of lath shaped particles in SEM confirmed the XRD data of no or little illite in our samples.

Elemental analysis by EDS with SEM, with a spatial resolution of approximately 5  $\mu\text{m}$  diameter indicated similar elemental peaks in the coating material from spot to spot on a single grain, and between coatings on different grains including coatings on feldspar, quartz, and Fe–Ti oxides. However, the EDS peak intensities vary. Semi-quantitative EDS analyses using the Philips EM420 microscope (TEM), with a spatial resolution of 2–10 nm show considerable compositional variability (Table 2 and Fig. 6). These analyses were collected from coating materials in four core samples, and include coatings on quartz and feldspars. The large variation in chemical composition indicates a mixture of coating mineral phases within the beam sampling volume as well as inadvertent sampling of the underlying or remnant feldspars.

#### 4.3. Surface morphology of feldspar grains

The morphology of feldspar surfaces was examined using FEG-SEM after the coating materials were removed ultrasonically. Fig. 7 displays the detailed examination of one feldspar grain. The round shaped K-feldspar has two visible pits, which are oval- or almond-shaped, and about 20  $\mu\text{m}$  in diameter along the long axis (Fig. 7a and b). While the etch-pits maintain an overall gently curving surface, a closer examination with increasing magnification shows angular and prismatic features at nanometer scale (Fig. 7c and d). The gently curved surfaces at low magnification are populated with angular prisms, all pointing in the same direction and perpendicular to the bottom of the oval-shaped pit surface, probably along the *c*-axis of the cleavages. Within the pits, steps are clearly developed. These terraces are about 500 nm long.

The prisms display sharp edges, and have a width of 500 nm to 1  $\mu\text{m}$ . The top of the prisms are almost at right angles to the sides. The sides of the prism surfaces are generally smooth, but also show elongated, straight or slightly curved cracks. The crack etch-pits have micron to sub-micron length and a width of a few nanometers. The directions of these crack etch-pits are parallel to the prisms, both along the long axis. These etch pits appear to resemble those crack-etch pits described by Berner and Holdren (1979), who attributed them to the initial stage of feldspar dissolution. However, these features are present only at a much finer scale in our study. Similar parallel-sided channels were found in weathered olivine, pyroxenes, pyroxenoids, amphiboles, and layer silicates, as well as feldspars (see summary of Banfield’s work in, Hochella and Banfield, 1995). Hochella and Banfield (1995) attributed these etch channels to the incipient stage of silicate mineral weathering, and noted the different properties of water and solution chemistry in these confined spaces as compared to the bulk aqueous solution.

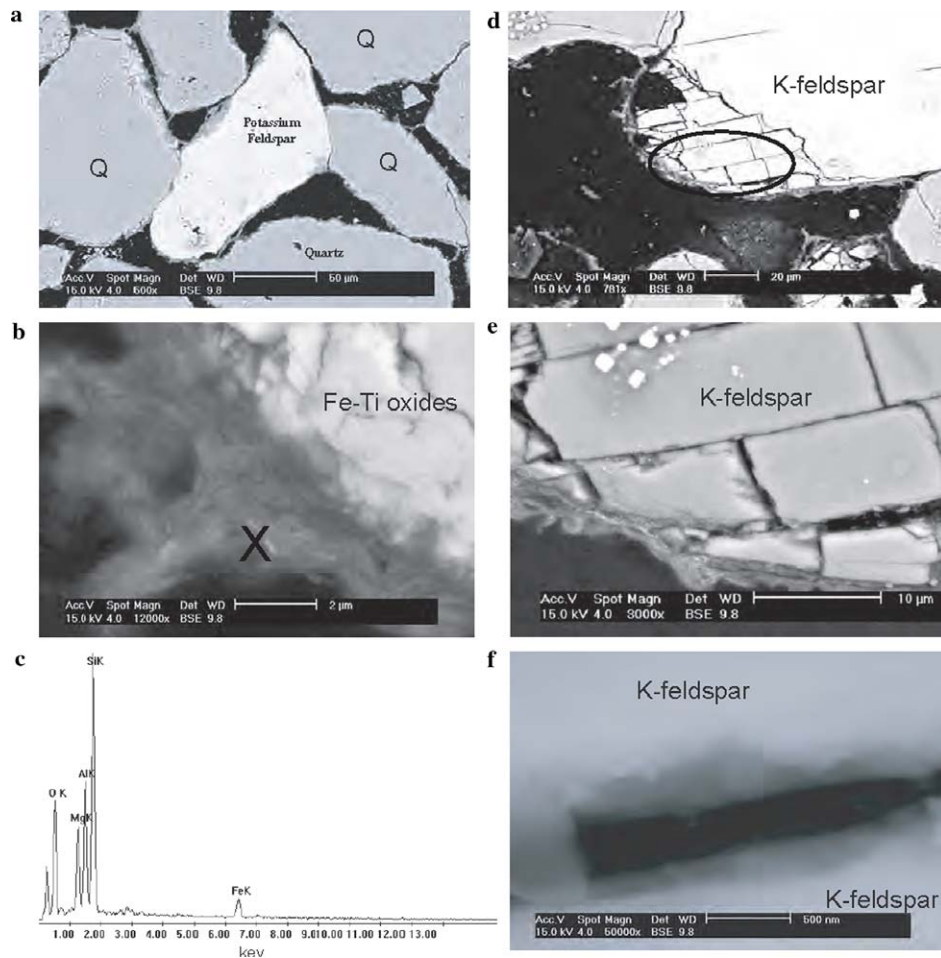


Fig. 4. SEM observations of Navajo Sandstone thin sections. (a) Electron micrograph of K-feldspar grain and coating materials. Q stands for quartz; (b) Coating layer formed on a Ti-Fe oxide; (c) EDS spectrum of the coating materials around Ti-Fe oxides, sampled in and around the area marked with "X" in (b); (d) A layer of coating is formed around cleaved K-feldspar. (e) An enlargement of the circled area in (d). Clayey materials have developed along the cleavage and part of the feldspar along the cleavage dissolved. (f) A close-up look of the opened cleavage (dark area).

The relatively "smooth" looking part of the grain at low magnification (see Fig. 7a) is covered with kaolin platelets (Fig. 7e). Hexagonal shape and sharp edges are seen in most platelets. All platelets have their basal plane aligned with the feldspar surface. The kaolinite adheres tightly to the feldspar surface. We used an ultrasonic probe to sonicate the samples for 45 min while keeping the sample in icy water to prevent overheating. Despite this treatment, the kaolinite platelets still remain on the feldspar surfaces when examined with SEM (Fig. 7i-k). This characteristic was observed repeatedly: the kaolinite adheres tightly to the feldspar surface while smectite was readily removed during sonication or even by washing. However, in all samples examined, kaolinite platelets did not form a continuous layer, and only developed on part of the feldspar grain surface.

The discontinuous cover pattern of the kaolinite may be attributed to three different causes: (1) this represents the original growth pattern of the kaolinite; (2) the kaolinite was originally covered on the whole surface of the feldspar, but was partly dissolved during the stage at which the

smectite precipitated; and (3) the kaolinite originally covered on the whole surface of the feldspar, but was partly or selectively removed during sonication and/or sample preparation.

In addition to coatings, K-feldspar overgrowth was also observed on detrital feldspar grains (Fig. 7f and g). The overgrowth shows perfect cleavages. An EDS profile shows Si, Al, K, and O peaks, but no Na peak while the detrital K-feldspar contains albite solid-solution (~5% from both electron microprobe and SEM/EDS). Authigenic overgrowths typically have subtle differences in mineral chemistry and crystallography from the substrate grains, and are often more stable than detrital feldspars. In some cases, a rind of diagenetic overgrowth is intact while detrital feldspars are dissolved away (Worden and Burley, 2003).

#### 4.4. Possible implications of coatings on feldspar dissolution kinetics

As pointed out by Hodson (2003), surprisingly little research has been carried out on the effects of surface coat-

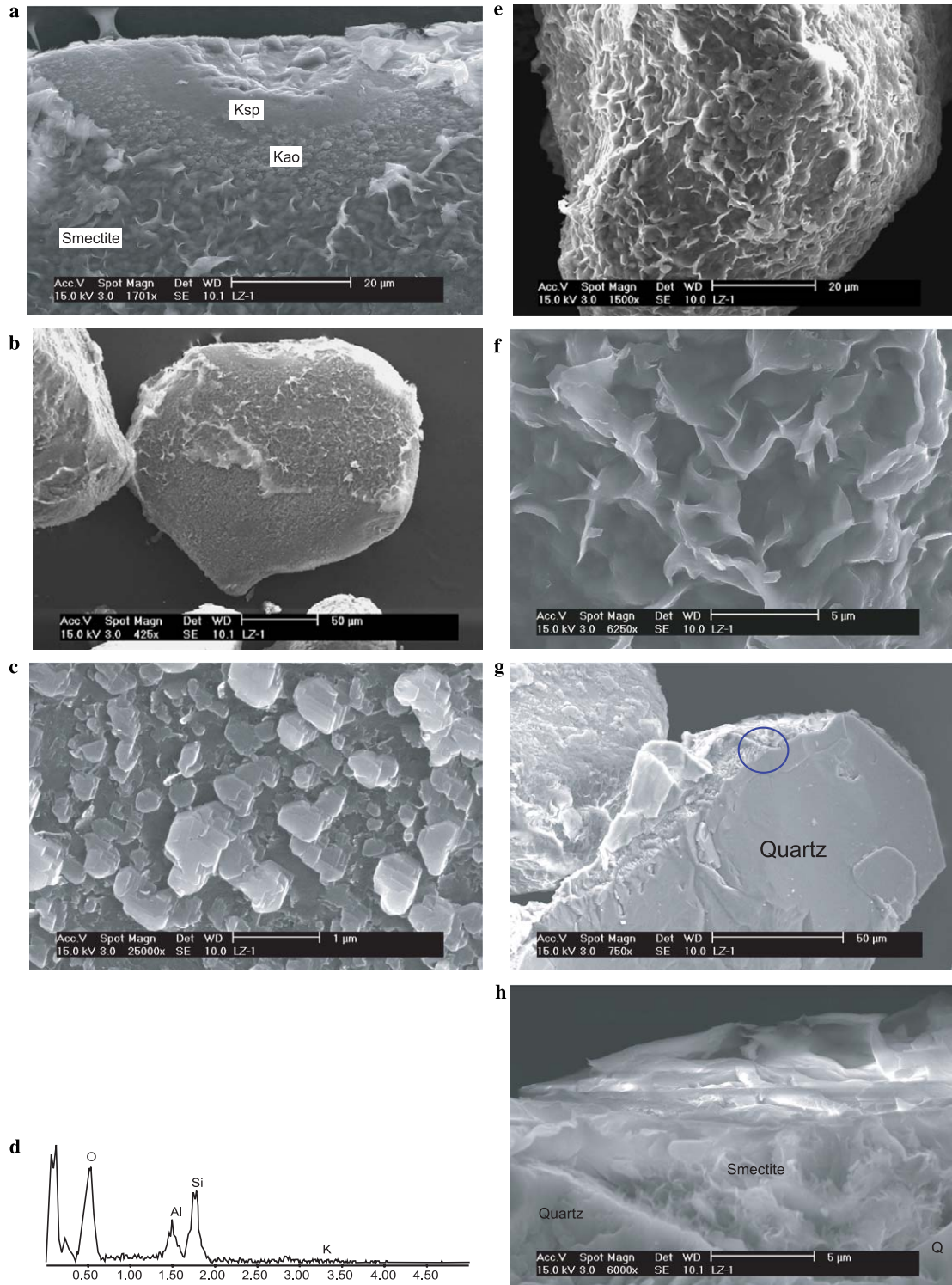


Fig. 5. SEM micrographs of grain-mounted Navajo Sandstone drill core. (a and b) Three layer “onion”. The grain is K-feldspar, and is coated with a layer kaolin platelets. Smectite in turn covers kaolin. (c) Euhedral to semi-euhedral hexagonal kaolin plates. (d) EDS spectrum of kaolin platelets. (e) A sediment grain covered with smectite. (f) High-resolution view of smectite in (e). (g) A quartz grain covered by smectite. (h) High-resolution view of smectite coating encircled in (g).

ings on mineral dissolution kinetics, despite the vastness of literature on silicate kinetics. Most citations of this topic were hypotheses and postulations. Petrovic (1976) and Helgeson (1971) reviewed earlier batch reactor laboratory

experiments, which ranged from room temperature to about 200 °C, pH from acidic to near neutral, and various starting solution compositions. These laboratory dissolution experiments produced only scarcely populated precip-

Table 2  
TEM/EDS analyses of the coating materials on sediment grains

Samples	SiO <sub>2</sub>	MgO	Al <sub>2</sub> O <sub>3</sub>	K <sub>2</sub> O	MnO <sub>2</sub>	Fe <sub>2</sub> O <sub>3</sub>	CaO	TiO <sub>2</sub>	Na <sub>2</sub> O	Total (%)
MSE-1	0.402	0.217	0.177	0.002	0.003	0.205	0.009	0.002	0.000	102
	0.383	0.211	0.206	0.001	0.003	0.220	0.002	0.003	0.000	103
	0.376	0.193	0.215	0.002	0.002	0.237	0.000	0.001	0.000	103
	0.693	0.000	0.209	0.104	0.000	0.001	0.004	0.000	0.005	102
	0.718	0.000	0.215	0.074	0.002	0.000	0.005	0.000	0.000	101
	0.637	0.036	0.188	0.045	0.007	0.089	0.003	0.000	0.000	101
	0.515	0.141	0.004	0.001	0.005	0.160	0.181	0.012	0.000	102
	0.537	0.008	0.385	0.003	0.000	0.043	0.020	0.000	0.005	100
	0.472	0.073	0.231	0.105	0.002	0.091	0.020	0.008	0.000	100
	0.572	0.073	0.193	0.034	0.000	0.126	0.010	0.005	0.000	101
	0.623	0.066	0.184	0.028	0.000	0.096	0.004	0.002	0.000	100
	0.510	0.131	0.187	0.009	0.003	0.170	0.008	0.000	0.000	102
	0.626	0.050	0.235	0.024	0.001	0.060	0.008	0.002	0.000	101
0.428	0.157	0.209	0.001	0.000	0.217	0.011	0.000	0.000	102	
MSE-2	0.402	0.217	0.177	0.002	0.003	0.205	0.009	0.002	0.000	102
	0.383	0.161	0.182	0.001	0.000	0.278	0.000	0.010	0.000	101
	0.343	0.059	0.132	0.004	0.005	0.458	0.006	0.001	0.000	101
	0.677	0.042	0.177	0.013	0.004	0.078	0.010	0.001	0.000	100
	0.651	0.054	0.207	0.010	0.000	0.071	0.011	0.000	0.000	100
	0.677	0.042	0.177	0.013	0.004	0.078	0.010	0.001	0.000	100
	0.406	0.161	0.205	0.003	0.002	0.236	0.005	0.000	0.000	102
	0.434	0.174	0.216	0.007	0.003	0.180	0.003	0.000	0.000	102
	0.434	0.174	0.216	0.007	0.003	0.180	0.003	0.000	0.000	102
	0.404	0.167	0.170	0.003	0.003	0.264	0.004	0.002	0.000	102
	0.421	0.144	0.191	0.004	0.003	0.244	0.009	0.000	0.000	102
	0.416	0.183	0.206	0.005	0.002	0.206	0.004	0.001	0.000	102
	0.432	0.051	0.152	0.037	0.003	0.323	0.004	0.008	0.000	101
	0.453	0.044	0.156	0.045	0.003	0.286	0.009	0.009	0.000	101
	0.641	0.048	0.215	0.040	0.001	0.043	0.017	0.000	0.000	100
	0.402	0.199	0.192	0.004	0.003	0.215	0.005	0.000	0.000	102
0.330	0.137	0.171	0.002	0.009	0.366	0.000	0.001	0.000	102	
MSE-3	0.404	0.218	0.179	0.002	0.003	0.206	0.009	0.002	0.000	102
	0.410	0.201	0.225	0.000	0.000	0.173	0.009	0.002	0.000	102
	0.661	0.048	0.212	0.011	0.000	0.042	0.024	0.000	0.004	100
	0.584	0.069	0.213	0.024	0.000	0.096	0.016	0.000	0.003	100
	0.347	0.201	0.225	0.000	0.002	0.243	0.011	0.000	0.000	103
	0.453	0.168	0.219	0.000	0.001	0.185	0.008	0.006	0.000	104
	0.618	0.060	0.251	0.015	0.000	0.028	0.030	0.008	0.000	101
	0.620	0.063	0.206	0.051	0.010	0.051	0.024	0.000	0.000	103
	0.660	0.044	0.211	0.015	0.000	0.046	0.020	0.000	0.011	101
	0.590	0.076	0.199	0.040	0.003	0.072	0.017	0.000	0.010	101
	0.595	0.058	0.201	0.054	0.001	0.066	0.024	0.001	0.002	100
	0.482	0.146	0.261	0.001	0.000	0.132	0.012	0.001	0.000	103
	0.616	0.058	0.209	0.044	0.000	0.060	0.017	0.002	0.000	101
	0.319	0.162	0.176	0.000	0.009	0.324	0.011	0.000	0.008	101
0.432	0.142	0.194	0.002	0.004	0.241	0.007	0.000	0.000	102	
0.509	0.138	0.224	0.007	0.002	0.139	0.005	0.000	0.000	102	
MSE-4	0.402	0.217	0.177	0.002	0.003	0.205	0.009	0.002	0.000	102
	0.603	0.064	0.220	0.071	0.006	0.047	0.011	0.000	0.000	102
	0.652	0.048	0.224	0.032	0.000	0.025	0.015	0.002	0.002	100
	0.506	0.098	0.195	0.011	0.000	0.190	0.017	0.000	0.000	102
	0.508	0.134	0.269	0.000	0.002	0.085	0.018	0.004	0.000	102
	0.428	0.179	0.210	0.004	0.004	0.188	0.003	0.000	0.000	101
	0.662	0.052	0.213	0.014	0.000	0.025	0.027	0.002	0.004	100
	0.613	0.072	0.207	0.054	0.005	0.016	0.023	0.003	0.007	100
	0.574	0.042	0.246	0.081	0.001	0.047	0.006	0.007	0.002	101
	0.379	0.184	0.210	0.006	0.002	0.210	0.015	0.003	0.000	101
	0.454	0.176	0.276	0.000	0.000	0.098	0.009	0.000	0.000	101
	0.478	0.028	0.326	0.107	0.001	0.035	0.007	0.010	0.009	100
	0.483	0.028	0.320	0.109	0.001	0.036	0.005	0.013	0.005	100
	0.413	0.119	0.150	0.086	0.003	0.219	0.003	0.019	0.000	101
	0.601	0.064	0.222	0.052	0.003	0.038	0.020	0.000	0.000	100



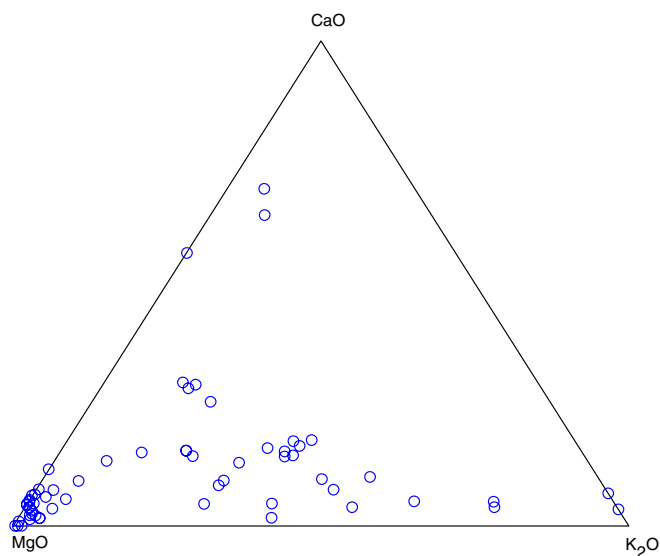


Fig. 6. Semi-quantitative chemical analyses (TEM-EDS) of coating materials on feldspars and quartz grains. The sampled volume apparently contains a mixture of various coating mineral phases as well as the underlying quartz and feldspars, which contributed to the large composition variation.

itates on dissolving grains; never was a continuous precipitate layer found on laboratory samples. Incongruent dissolution of feldspars resulted in precipitation of boehmite, kaolinite, smectite, and their disordered and poorly crystallized analogs, although limitations of electron microscopic techniques in 1960s and earlier cast doubts on the accuracy of the presented mineral identifications in some earlier studies. However, all laboratory experiments were short, ranging from a few hours to 2 years, and were conducted with static flow conditions (batch experiments). From these experiments, Petrovic (1976) concluded that secondary precipitates did not constitute a diffusional barrier.

Nugent et al. (1998) buried albite slabs in acidic soils for up to 3.5 years. They found patchy amorphous looking materials after as short as half a year. However, their field experiment was still short as for geological processes. They alluded to the possible inhibitive effects of the coatings, but did not elaborate on possible mechanics.

As described above, all feldspar grains in the Navajo Sandstone at Black Mesa were partially covered with kaolin platelets and a continuous layer of smectite. A continuous coating on sediment grain surface also occurs in the Atlantic Coastal Plain sediments (Penn et al., 2001) and in the Santa Fe Aquifer, Pajarito Plateau, north-central New Mexico (Hereford et al., 2005). Similarly, coatings on soil grains are common (Hodson, 2003, and references cited therein). In contrast, a continuous coating layer that envelops the feldspar grains by secondary minerals has never been replicated in the laboratory or field experiments. The wide occurrences of a coating layer on naturally weathered silicates may indicate that clay coating from feldspar weathering is ubiquitous because, over geological time, feldspar dissolution is incongruent. Therefore, the

presence of coatings on feldspars in nature represents a condition that departs from the laboratory experiment condition of pristine mineral grain surfaces.

Most discussions of the coatings on primary silicate have centered on the possibility that the coating layer represents a diffusional barrier (Helgeson, 1971; Petrovic, 1976; Berner and Holdren, 1979). Besides diffusion, the secondary precipitates on feldspars may affect feldspar dissolution in other ways. Cubilas et al. (2005) conducted coupled  $\text{CaCO}_3$  dissolution –  $\text{CdCO}_3$  precipitation experiments, and found that the precipitation of a layer ( $\sim 10$  nm thick) of otavite ( $\text{CdCO}_3$ ) reduced calcite dissolution rates by close to two orders of magnitude. On the other hand, otavite precipitation on aragonite, ground clam, mussel, and cockle shell did not reduce  $\text{CaCO}_3$  dissolution rate. Even though the otavite coating layer on calcite is not perfectly continuous, it nevertheless reduces calcite dissolution rate; fine gaps are visible in the surface coating layer.

Similar effects of kaolin coatings on feldspar may reduce dissolution rates in the Navajo Sandstone at Black Mesa, where kaolin platelets strongly adhere onto feldspar grain surface, with their (001) basal plane aligned parallel to the feldspar surface. Such strong bonds or tight adhesion between the two particles suggest some structural connections during nucleation. These connections may block the feldspar reaction sites on the surface or effect a reduction of the effective reactive surface area.

Cubilas et al. (2005) attributed the negligible effects of otavite coating on aragonite to the formation of a randomly stacked, porous, three-dimensional layer, which does not block surface sites or diffusion. Similarly, Hodson (2003) showed, experimentally, that the presence of porous Fe oxides coatings does not affect the dissolution of anorthite. The porous smectite layer in the Navajo Sandstone at Black Mesa, although generally continuous, is porous, and behaves in a similar fashion. The smectite layer is nevertheless a part of the feldspar dissolution story through the connection with the chemical reaction network (Zhu et al., 2004).

It is commonly stated in the literature that the red Navajo Sandstone has an iron oxyhydroxide layer sandwiched between feldspar and quartz grain, and the clay coating. It has been further argued that the positively charged iron oxyhydroxides bind the negatively charged feldspar/quartz and negatively charged clay minerals (Swartz et al., 1997). However, it was shown that the reddish looking coatings on sediment grains in Atlantic Coastal Plain do not have a thin iron oxyhydroxide layer, although it appears so under polarized light microscope (Penn et al., 2001). The current study observed similar absence of the purported iron oxyhydroxide layer. Iron oxyhydroxides in the Navajo Sandstone are disseminated in the clay coating and apparently do not affect feldspar dissolution.

It is certainly intriguing that kaolinite only developed on feldspar grains whereas smectite covers on all sorts of sed-

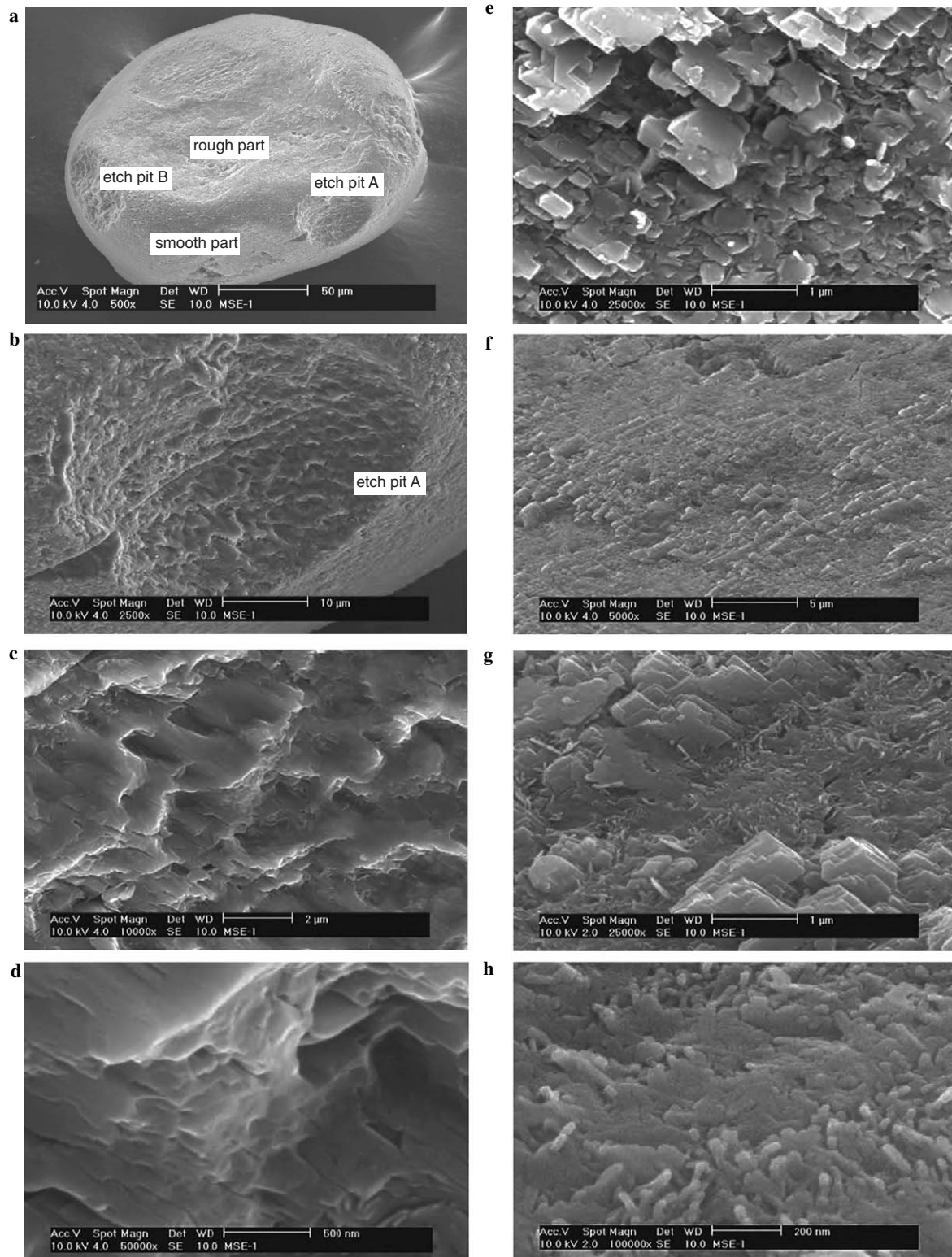


Fig. 7. SEM micrographs of feldspar grains. Smectite coating was removed by ultrasonification. (a) A feldspar grain after sonication with a sonic probe. (b) Etch pit A in (a); (c) Higher resolution of (b), showing dissolution features; (d) Still higher resolution of (b); (b–d) show feldspar surface that is not covered by smectite or kaolinite. (e) Kaolin plates on the “smooth” part of the grain in (a); (f) and (g) “rough” part in (a), showing K-feldspar overgrowth “outcrops,” which shows cleavage well. The edges are very sharp. The identification of feldspar was confirmed by EDS with Si, Al, K, and O peaks on the well cleaved grains; (h) Smectite still adhered to the K-feldspar surface. (i) Kaolinite remained on a feldspar grain after the sample were vigorously sonicated with a sonic probe for 45 min. They look like sugar coating on donuts. (j) Enlarged view of (i). (k) Another feldspar grain covered with kaolinite. The sugar coating looking particles are kaolinite.



Fig. 7 (continued)

iment grains. While kaolinite can derive all its constituents (Al, Si) from feldspar dissolution, smectite needs additional constituents (K, Na, Ca, Mg, and Fe) transported by groundwater. In general, diffusion in aqueous solution is fast with respect to precipitation rate that the characteristic distance of diffusion, which determines the spatial spread of the precipitates or the mean distance of transport of the precipitating component (Crank, 1975; Petrovic, 1976), is long under aquifer conditions. Applying the mathematical solutions provided by Crank (1975) and Petrovic (1976), we can show, qualitatively, that if kaolinite precipitation is instantaneous with respect to the feldspar dissolution rate at far from equilibrium but smectite precipitation is slow, a closely packed kaolinite can develop on feldspar surfaces while smectite precipitation is dispersed in the aquifer. This difference between kaolinite and smectite can also be triggered by different modes of crystal nucleation.

It also should be noted that kaolinite has its basal plane parallel to the feldspar grain surface in the Navajo Sandstone while kaolinite formed in the batch reactor experiments randomly stacked on feldspar surface

(Fig. 8, also see review of earlier work by Petrovic (1976)). The force of flowing groundwater near the grain surface may have made the difference. Reaction-path calculations show that the feldspar-water batch reactor system reaches equilibrium when only a small fraction of feldspar is dissolved. Thus, an insufficient amount of kaolin or other secondary clay minerals were produced in the batch-reactor experiments to form a continuous clay layer or dense patches, as observed in the literature (Petrovic, 1976). In contrast, aquifers are dynamic systems, with fresh, unsaturated solution replenishing from upstream. The feldspar-clay-water systems are long-lived, and dense patches of kaolin and a continuous smectite layer formed.

#### 4.5. Amorphous surface layer

##### 4.5.1. HRTEM observations

HRTEM reveals a layer of amorphous materials that is ubiquitously present between the K-feldspar surface and clays (Figs. 9 and 10). The interface between crystalline feldspar and the amorphous layer is sharp. The



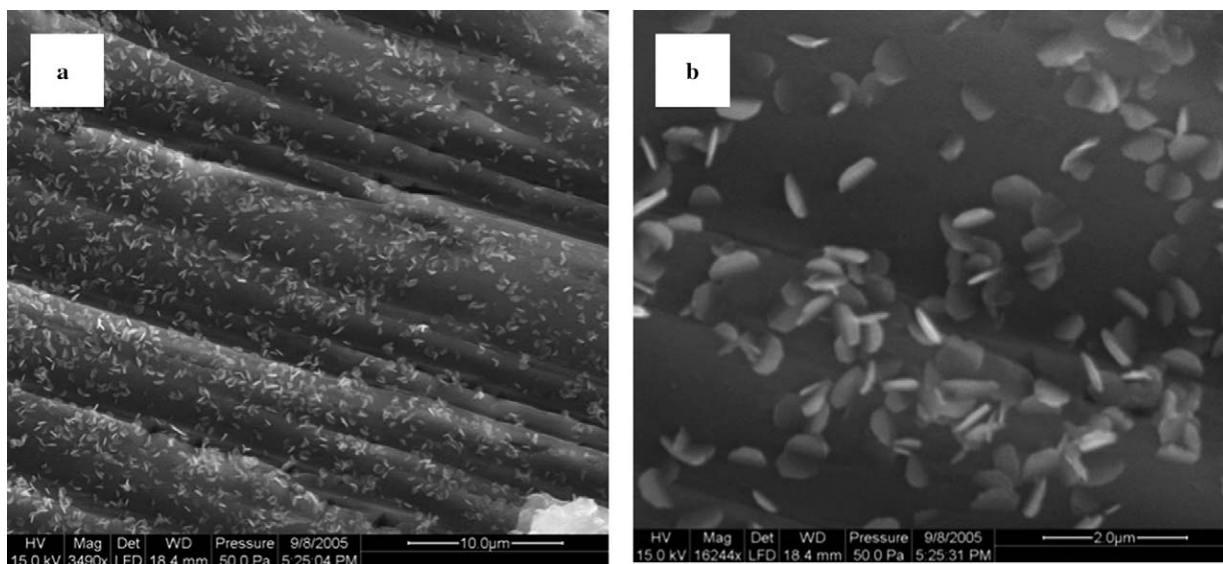


Fig. 8. Scanning electron microscopy images of microcline surface after batch reactor dissolution experiment. Crystalline kaolin, with the size of  $<0.5 \mu\text{m}$  and a shape of hexagons, are randomly stacked on feldspar surface. The random orientation is in direct contrast with the oriented kaolinite coatings in the Navajo Sandstone aquifer (cf. Fig. 4c). Experiment was conducted with a flexible reaction cell system at  $200^\circ\text{C}$  and 300 bars with a starting solution of 200 mM KCl and 50 mM  $\text{CO}_2$  and was ended after 27 days when the reaction products were examined. Experiment was performed by William Seyfried in collaboration with Chen Zhu.

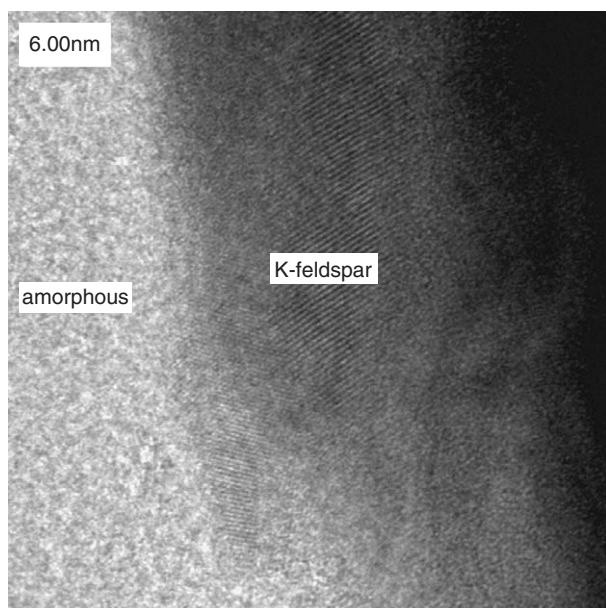


Fig. 9. TEM images of coexistence of K-feldspars and the electron diffraction amorphous layer.

thickness of the layer is thin, in most cases about 10 nm thick, but can be as thick as 50 nm. This was observed by multiple experimentalists, and was observed on all samples, which include samples with bright reddish color and white or grey colors (cf. Beitzler et al., 2005). While ion milling may produce an amorphous layer, the amorphous layer was also observed on crush-prepared samples. Thus, the amorphous layer is not a sample preparation artifact.

Complete compositional characterization of the amorphous layer was not successful because the amorphous layer is particularly susceptible to beam damage. There were some qualitative indications that the amorphous layer is deficient in K and enriched in Si with respect to the underlying unaltered feldspar. The lack of chemical composition data makes it difficult to determine whether the amorphous layer is a true chemically leached layer, or is a re-precipitation of detached silica (Hellmann et al., 2003), or is a re-polymerization and condensation layer (Casey et al., 1989a,b, 1993).

#### 4.5.2. Comparison with previous studies

Earlier workers postulated a preferentially leached residuum on the feldspar surface (e.g., depleted in interstitial cations Na, K, Ca, and framework element Al, and enriched in Si and H) from the non-stoichiometric dissolution behavior and parabolic solute release rates shown at the initial stage of dissolution (diffusion through a thickening secondary mineral layer will produce the same pattern of solute release behaviors; See Drever (1988) for a clear and concise discussion). During the course of the last twenty years, there have been many arguments and counter-arguments advanced over whether such a layer exists, based on various analytical techniques, the details of which we shall omit here but readers are referred to Blum and Stille (1995) and Brantley (2004). However, it has been generally agreed, until lately (see below), that this layer was confirmed by a variety of spectroscopic and ion beam techniques, mostly on laboratory leached feldspars in extremely acidic to acidic solutions (Schott and Petit, 1987; Casey et al., 1988; Hochella et al., 1988; Nesbitt and Muir, 1988; Casey et al., 1989a; Petit et al., 1989; Hellmann



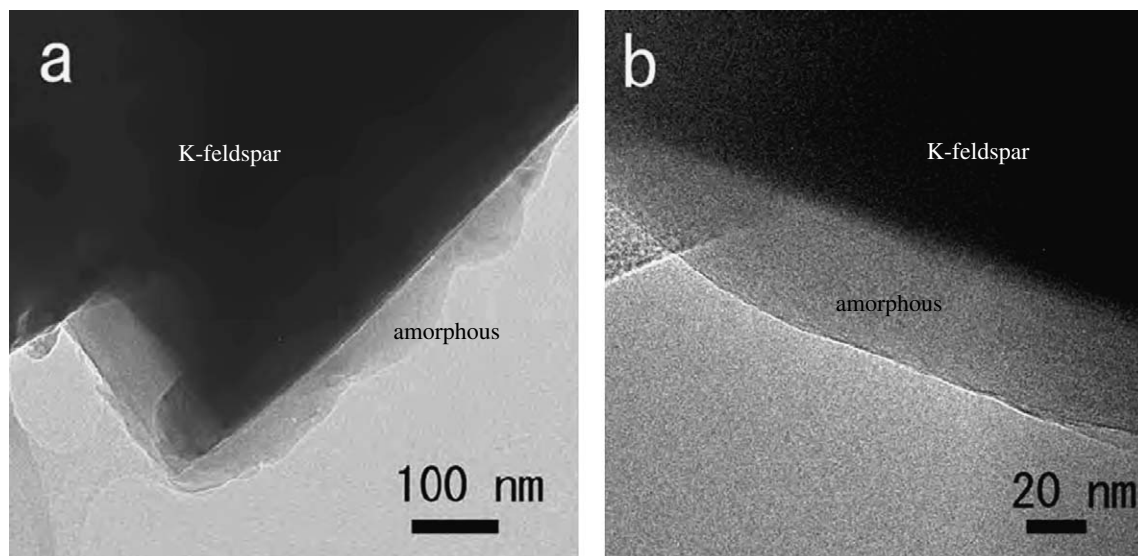


Fig. 10. TEM images of coexistence of K-feldspars and amorphous layers.

et al., 1990; Muir et al., 1990; Petit et al., 1990; Innskeep et al., 1991; Hellmann, 1997a; Nugent et al., 1998; Nesbitt and Skinner, 2001). A sigmoidal pattern of  $\text{Na}^+$ ,  $\text{Ca}^{2+}$ ,  $\text{Si}^{4+}$ , and  $\text{Al}^{3+}$  distribution with depth from the dissolved mineral surfaces was observed by a variety of surface analytical techniques (e.g., Nugent et al., 1998; Nesbitt and Skinner, 2001). The thickness of the residuum layer is a function of pH, temperature, and reaction time, and can be as thick as 100 nm (e.g., Nesbitt and Skinner, 2001). The thicknesses of the layer decrease with increasing solute concentrations and increase with decreasing pH.

The finding of a sigmoidal element distribution pattern with depth from feldspar grain surfaces has led to the “leached layer” hypothesis. During the formation of a leached layer, there are two reaction fronts: (1) advancement of the pristine feldspar-leached zone interface; and (2) dissolution of the leached layer at the edge of the solid phase or retreat of the mineral–water interface. This process has been modeled as a Fick’s Second Law problem with moving boundaries through the following advection–diffusion equation (Lasaga, 1998),

$$\frac{\partial C}{\partial t} = \frac{\partial C}{\partial x} \left( D \frac{\partial C}{\partial x} \right) + v \frac{\partial C}{\partial x}, \quad (1)$$

where  $C$  stands for the concentrations of a diffusing species ( $M/L^3$ ),  $D$  the diffusion coefficient ( $L^2/T$ ), or the interdiffusion coefficient (Hellmann, 1997b) in the leached layer,  $x$  the distance from fluid–mineral interface to the particle interior ( $L$ ), and  $-v$  the velocity of constituents moving toward the surface ( $L/T$ ).

This formulation has been used extensively in the glass corrosion literature (Doremus, 1967; Doremus, 1975; McGrail et al., 1984; Smets and Tholen, 1985), and has been adopted for interpreting the sigmoidal concentration profiles associated with the leached layer on feldspar surfaces (Brantley and Stillings, 1996; Hellmann, 1997b;

Lasaga, 1998; Nesbitt and Skinner, 2001; Hellmann et al., 2003). This approach postulates that preferential leaching from feldspars results in a parabolic rate law at the initial stage of the dissolution experiments. After a period of time, a steady state was reached such that the two reaction fronts have the same velocities, the thickness of the leached layer is constant, and the rate law becomes linear.

However, the development of a leached layer above pH 3 has not been positively observed (Brantley, 2004). In fact, it is believed that the leached layer is absent at basic pH (Holdren and Speyer, 1985; Casey et al., 1989a; Casey and Bunker, 1990; Schweda, 1990; Blum and Stillings, 1995). Consequently, two separate, pH-dependent feldspar dissolution pathways were postulated (Brantley and Stillings, 1996 also reviewed by Hellmann et al., 2003): (1) non-stoichiometric dissolution and near surface alteration at acidic to neutral pH; and (2) stoichiometric dissolution and absence of near-surface alteration at basic pH.

Even the development of a truly leached layer in acidic solutions for laboratory experiments has been challenged recently. Hellmann et al. (2003, 2004), based on HRTEM and Energy-filtered TEM (EFTEM) data, questioned the leached origin of the surface layer and suggested a dissolution-reprecipitation mechanism. Their arguments are mainly based on the sharp chemical gradients found across the crystalline feldspar–amorphous layer interface which, they contend, cannot be explained by the advection–diffusion–reaction model of Eq. (1). They further assert that the observed sigmoidal compositional variations with depth from the feldspar grain surface are artifacts of surface analytical methods (Hellmann et al., 2004). However, Nesbitt and Skinner (2001) carefully used unreacted feldspars as references for comparison with reacted feldspars, which they felt corrected any analytical artifacts.

The presence or absence of an amorphous layer on feldspar surfaces is significant to theories of surface reaction-

controlled feldspar dissolution mechanism(s). Earlier work suggests that the leached layer may form a diffusional barrier, but the current thinking is that silicate dissolution is controlled by surface reactions (Lagache et al., 1961a; Lagache et al., 1961b; Lagache, 1965; Lagache, 1976; Aagaard and Helgeson, 1982; Murphy and Helgeson, 1987; Blum and Lasaga, 1988; Drever, 1988; Blum and Lasaga, 1991; Oelkers, 2001; Brantley, 2004). The question of “what feldspar surface” is therefore critical in any surface-reaction controlled mechanism.

#### 4.5.3. Postulation of the origin of amorphous layer at Black Mesa

The amorphous layer on our naturally weathered K-feldspars at Black Mesa is currently in contact with alkaline (pH up to ~9) groundwater. From the solute fluxes in the aquifer, it is postulated that the feldspars in the saturated Navajo Sandstone are dissolving at a very slow rate (Zhu, 2005). If the amorphous layer is indeed a leached layer and is related to the current groundwater, and a steady-state is reached between the dissolution front and the leaching front, the characteristic thickness ( $\tau$ ) of the leached layer can be estimated following Lasaga (1998). For single solute diffusion with uniform and concentration-independent diffusion coefficients,

$$\tau = \frac{D}{v}. \quad (2)$$

Eqs. (1) and (2) represent single solute diffusion. Multicomponent diffusion would be more representative of the situation (Hellmann, 1997b). Our observed thickness of the amorphous layer is approximately 10 nm or  $10^{-8}$  m. The derived dissolution rate of K-feldspar of  $10^{-18.8}$  mol m<sup>-2</sup> s<sup>-1</sup> (Zhu, 2005) translates into a  $v$  of  $2 \times 10^{-23}$  m s<sup>-1</sup> if we assume the molar volume of feldspars is  $\sim 100$  cm<sup>3</sup>/mol. Eq. (2) gives a  $D$  value of  $10^{-27}$  cm<sup>2</sup> s<sup>-1</sup>. Hellmann (1995) shows that Na<sup>+</sup> diffusion coefficients is  $10^{-34}$  cm<sup>2</sup> s<sup>-1</sup> for crystalline albite and  $10^{-12}$  cm<sup>2</sup> s<sup>-1</sup> for albite glass at 25 °C when experimental data at 200–300 °C were extrapolated to room temperature.

An extremely small diffusion coefficient apparently contradicts some previous experimental studies of leached layer in acidic solutions, which point to the formation of a porous, hydrous, amorphous silica layer under acidic conditions. One possible reconciliation of the apparent conflict is that a leached layer may be present beneath the reported porous amorphous layer but cannot be resolved except with high-resolution electron microscopy. This has been observed for glass weathering in radioactive slag (Linda Veblen, personal communication). A thick, porous, crumbly layer, comprised of mostly amorphous silica and iron oxyhydroxides, forms a residuum on weathered slag as a result of 30 years' weathering. Beneath this layer lies a leached zone with parabolic distribution of U, Th, and REE. In this case, the glass dissolution rate far outpaces the amorphous silica dissolution rate.

At pH above ~3, alkali feldspar dissolution rates are slower than the silicon-normalized amorphous silica dissolution rate at 25 °C (Blum and Stillings, 1995). Conceptually, silica tetrahedra will detach from the leached layer edge at a faster pace than the advancement of the leaching front into the pristine feldspar interior. A very thin silica-rich amorphous layer will form, or no layer at all. As we emphasized repeatedly, a nanometer-thick leached layer can only be detected with high resolution techniques.

#### 4.6. Paragenesis, surface features, and coating minerals

The obvious advantage of the study of silicate surfaces in aquifers is that these mineral surfaces have reacted with fluids for a long period of time, which cannot be replicated in the laboratory. However, the observed surface features may result from a number of indistinguishable overprinting events and processes: (1) erosion and weathering; (2) fluvial and aeolian transport of the sediment grains; (3) earlier diagenesis; (4) burial diagenesis; and (5) multiple events during “uplift diagenesis”. Particularly, basin scale fluid flow must have played a significant role in burial diagenesis or uplift diagenesis. Beitler et al. (2005) related the various colors of the Navajo Sandstone to the migration of reducing and bleaching fluids through the fault systems. If this occurred at Black Mesa, it indicates an episode of acidic fluids and intense alteration of feldspars.

A complete reconstruction of diagenetic history for the Navajo Sandstone at Black Mesa is beyond the scope of this study. Below, we give a brief discussion of the paragenetic sequences and possible relationships with feldspar dissolution kinetics. Both Net (2003) and Beitler et al. (2005) described the diagenetic history of Navajo Sandstones in Wyoming and Utah, but they noticed that burial depths and diagenetic history vary significantly with location.

The Navajo Sandstone sediments may have been recycled before. However, aeolian transport involves effective abrasion so that earlier weathering features on grain surfaces such as clay coating and/or amorphous layers would not survive (Whalley et al., 1987), although the recycling may have generated internal porosity in both feldspars and quartz as is seen in electron microscopy in our study. Thus, the surface of aeolian feldspar grains was probably “fresh” before diagenesis. Worden and Burley (2003) divided sandstone diagenesis into three conceptual regimes associated with the stages of sedimentary basin evolution: early diagenesis (eogenesis), burial diagenesis (mesogenesis), and uplift-related diagenesis.

The etch pits, kaolinite, and smectite coatings could have been developed during any of the three stages. However, smectite is the outermost layer of the coatings, covering kaolinite, etch pits, K-feldspar overgrowth, amorphous layer on feldspars, and quartz overgrowth. Therefore, it is clearly a later product with respect to the others. Smectite penetrates feldspar crevices and unweathered feldspar remnants are embedded in the smectites (see Fig. 4). Thus, smectite is no doubt a weathering

product of feldspars in our samples, not the result of what is often referred to in the literature as “mechanical infiltration” (Mucke, 1994). At Black Mesa, very little to no illite is found, indicating that smectite was either never converted to illite or that illite is nearly completely consumed in earlier reactions.

Although the “contemporary” groundwater, from which feldspar dissolution rates were derived (Zhu, 2005), may not be responsible for part or all of the observed etch pits, amorphous layer, kaolinite coatings, and smectite coatings, these surface characteristics are the intrinsic properties of feldspar that represent their reactivity, whether or not they are relic. If the dilute recharging groundwater is undersaturated with respect to feldspars, feldspars shall dissolve. Dissolution of feldspars would lead to kaolinization and further formation of smectite if the supplies of other cations from groundwater fluxes are available. The reaction sequence is still *feldspar* → *kaolinite* → *smectite* (Helgeson, 1971; Helgeson and Murphy, 1983), provided that the solution chemistry is right.

## 5. Conclusions and remarks

Due to their significance in environmental and geological processes, silicate dissolution rates have been determined in a vast number of laboratory experiments. However, nearly all the experiments measured the dissolution of freshly ground powders with pristine surfaces. Here, we show that the “aged” feldspar surfaces in the Jurassic Navajo Sandstone at Black Mesa have onion like layers that modified their properties. Therefore, the differences in reactivity between feldspar grains in geological systems and laboratory experiments may represent one different “intrinsic” condition in the field and laboratory, which contributes to the observed orders of magnitude apparent discrepancy between field and laboratory dissolution rates. Field emission gun scanning electron microscopy (FEG-SEM), associated energy dispersive X-ray spectroscopy (EDS), and high resolution transmission electron microscopy (HRTEM) analytical electron microscopy (AEM) show the following features of the surface of the “aged” feldspar grains:

(1) All K-feldspar grains have a thin (~10 nm) amorphous layer, which is possibly enriched in Si and deficient in K. This amorphous layer is currently associated with slightly alkaline to alkaline groundwater. Because the nanometer thick amorphous layer can only be detected with high resolution TEM, but not with optical microscope or SEM, how widely it occurs on feldspars that have been weathered over geological time is not known. The origin of this amorphous layer and the possible roles of the amorphous layer are unknown. Nevertheless, this amorphous layer must be considered in dissolution mechanisms and rate laws if it widely occurs in nature. We are vigorously pursuing this subject with theoretical, laboratory experiments, and spectroscopic studies.

- (2) We found authigenic K-feldspar overgrowth and tightly adhered kaolin on K-feldspar surface, both of which reduce feldspar reactivity, but these coatings are not continuous and it is doubtful that they alone have caused five orders of magnitude reduction in dissolution rates (Zhu et al., 2004; Zhu, 2005).
- (3) A 3–5 μm thick smectite layer coats the feldspar grains continuously, but this layer is porous and does not constitute a diffusion barrier.

A major advancement in the last 40 years in our understanding of feldspar dissolution kinetics is the recognition of the critical importance of feldspar-water interface and surface reactions. This study raised the question, “What is the feldspar-water interface?” Resolution of this ambiguity of the interface(s) is central to the quantification of heterogeneous reaction kinetics in geological systems.

## Acknowledgments

C.Z. acknowledges the National Science Foundation for support of this research (EAR-0003816, 0423971, and 0509775). Core and drill cutting samples were provided by the Department of Energy’s Grand Junction Office and the Arizona Geological Survey. We thank Yang Ding, Barbara Osgood, Peng Lu, and Hiromi Konishi for some TEM and SEM images, Chusi Li for electron microprobe analysis, and Steven Chipra for the XRD analysis. We also thank Brenda Beitler and Laura Net for providing unpublished manuscripts and thesis, respectively. Discussion with Earle McBride, David Bish, and Arndt Schimmelmann was helpful. Editing by Corinne Shirley and various assistance from Angela Xu, Tracee Imai, Peng Lu, and Dana McClish is appreciated. C.Z. thanks Bill Seyfried for his permission to publish Fig. 8 ahead of the publication of their collaborated research.

Associate editor: Johnson R. Haas

## References

- Aagaard, P., Helgeson, H.C., 1982. Thermodynamic and kinetic constraints on reaction rates among minerals and aqueous solutions. I. Theoretical considerations. *Am. J. Sci.* **282**, 237–285.
- Aronson, J., Buntner, R.L., 1983. K/Ar dating of illite clays in Jurassic Nugget Sandstone and timing of petroleum migration in Wyoming overthrust belt. *AAPG Bull.* **67**, 414.
- Beitler, B., Parry, W.T., Chan, M.A., 2005. Fingerprint of fluid flow: chemical diagenetic history of the Jurassic Navajo Sandstone, southern Utah, USA. *J. Geophys. Res.* **75** (4), 547–561.
- Berner, R.A., Holdren, G.R., 1979. Mechanism of feldspar weathering-II. Observations of feldspars from soils. *Geochim. Cosmochim. Acta* **43**, 1173–1186.
- Blakey, R.C., Peterson, F., Kocurek, G., 1988. Synthesis of late Paleozoic and Mesozoic eolian deposits of the western interior of the United States. *Sediment. Geol.* **56**, 3–125.
- Blum, A.E., Lasaga, A.C., 1988. Role of surface speciation in the low-temperature dissolution of minerals. *Nature* **4**, 431–433.
- Blum, A.E., Lasaga, A.C., 1991. The role of surface speciation in the dissolution of albite. *Geochim. Cosmochim. Acta* **55**, 2193–2201.

- Blum, A.E., Stillings, L.L., 1995. Feldspar dissolution kinetics. In: White, A.F., Brantley, S.L. (Eds.), *Chemical Weathering Rates of Silicate Minerals*, vol. 31. Mineralogical Society of America, USA, pp. 291–346.
- Brantley, S.L. 1992. Kinetics of dissolution and precipitation-experimental and field results. in: *Proceedings of the Seventh International Conference on Water–Rock Interactions*, 7, pp. 465–469.
- Brantley, S.L., 2004. Reaction kinetics of primary rock-forming minerals under ambient conditions. In: Holland, H.D., Turekian, K.K. (Eds.), *Treatise on Geochemistry*, vol. 5. Elsevier, New York, pp. 73–117.
- Brantley, S.L., Stillings, L.L., 1996. Feldspar dissolution at 25 °C and low pH. *Am. J. Sci.* **296**, 101–127.
- Brown, J.G., Eychaner, J. H. 1988. Simulation of five ground-water withdrawal projections for the Black Mesa area, Navajo and Hopi Indian Reservations, Arizona, *US Geological Survey*, pp. 51.
- Buntner, R.L., Nigrini, A., 1994. Thermochronology of the Idaho–Wyoming thrust belt during the Sevier Orogeny: a new, calibrated, multiprocess thermal model. *AAPG Bull.* **78**, 1586–1612.
- Casey, W.H., Banfield, J.F., Westrich, H.R., McLaughlin, L., 1993. What do dissolution experiments tell us about natural weathering? *Chem. Geol.* **105**, 1–15.
- Casey, W.H., Bunker, B.C. 1990. The leaching of mineral and glass surfaces during dissolution. Chapter 10. In: Hochella, M., White, A. (Eds.), *Mineral–Water Interface Geochemistry*, pp. 397–426.
- Casey, W.H., Westrich, H.R., Arnold, G.W., 1988. Surface chemistry of labradorite feldspar reacted with aqueous solutions at pH—2, 3, and 12. *Geochim. Cosmochim. Acta* **52**, 2795–2807.
- Casey, W.H., Westrich, H.R., Arnold, G.W., Banfield, J.F., 1989a. The surface chemistry of dissolving labradorite feldspar. *Geochim. Cosmochim. Acta* **58**, 821–832.
- Casey, W.H., Westrich, H.R., Massis, T., Banfield, J.F., Arnold, G.W., 1989b. The Surface of labradorite feldspar after acid hydrolysis. *Chem. Geol.* **78**, 205–218.
- Chipera, S.J., Bish, D.L., 2002. FULLPAT: a full-pattern quantitative analysis program for X-ray powder diffraction using measured and calculated patterns. *J. Appl. Crystallogr.* **35**, 745–749.
- Cooley, M.E., Harshbarger, J.W., Akers, J.P., W.F. H. 1969. Regional hydrogeology of the Navajo and Hopi Indian Reservations, Arizona, New Mexico, and Utah. *US Geological Survey Professional Paper 521-A*, pp. 61.
- Crank, J., 1975. *The Mathematics of Diffusion*. Oxford University Press, Oxford.
- Cubillas, P., Kohler, S., Prieto, M., Causserand, C., Oelkers, E.H., 2005. How do mineral coating affect dissolution rates? An experimental study of coupled CaCO<sub>3</sub> dissolution—CaCO<sub>3</sub> precipitation. *Geochim. Cosmochim. Acta* **69** (23), 5459–5476.
- Doremus, R.H., 1967. *J. Non-Cryst. Solids* **19**, 137–144.
- Doremus, R.H., 1975. Interdiffusion of hydrogen and alkali ions in a glass surface. *J. Non-Cryst. Solids* **19**, 137–144.
- Drever, J.I., 1988. *The Geochemistry of Natural Waters: Surface and Groundwater Environment*. Prentice-Hall, Englewood Cliffs, New Jersey.
- Drever, J.I., Clow, D.W., 1995. Weathering rates in catchments. In: White, A.F., Brantley, S.L. (Eds.), *Chemical Weathering Rates of Silicate Minerals*, vol. 31. Mineralogical Society of America, USA, pp. 463–481.
- Dulaney, A.R. 1989. The geochemistry of the N-aquifer system, Navajo and Hopi Indian Reservations, Northeastern Arizona. Master thesis, Northern Arizona University, 209 p.
- Eychaner, J.H. 1983. Geohydrology and effects of water use in the Black Mesa area, Navajo and Hopi Indian Reservations, Arizona, *US Geological Survey Water Supply Paper 2201*, pp. 26.
- Harshbarger, J.W., Repenning, C.A., Irwin, J.H. 1957. Stratigraphy of the Uppermost Triassic and the Jurassic Rocks of the Navajo Country, *US Geological Survey Professional Paper 291*, pp. 71.
- Helgeson, H.C., 1971. Kinetics of mass transfer among silicates and aqueous solutions. *Geochim. Cosmochim. Acta* **35**, 421–469.
- Helgeson, H.C., Murphy, W.M., 1983. Calculation of mass transfer among minerals and aqueous solutions as a function of times and surface area in geochemical processes, I. Computational approach. *Math. Geol.* **15** (1), 109–130.
- Hellmann, R., 1995. The albite-water system; Part II, The time-evolution of the stoichiometry of dissolution as a function of pH at 100, 200, and 300 °C. *Geochim. Cosmochim. Acta* **59** (9), 1669–1697.
- Hellmann, R., 1997a. The albite-water system; Part III. Characterization of leached and hydrogen-enriched layers formed at 300 °C using MeV ion beam techniques. *Geochim. Cosmochim. Acta* **61**, 1575–1594.
- Hellmann, R., 1997b. The albite-water system; Part IV. Diffusion modeling of leached and hydrogen-enriched layers. *Geochim. Cosmochim. Acta* **61**, 1595–1611.
- Hellmann, R., Eggleston, C.R., Hochella, M.F., Crerar, D.A., 1990. The formation of leached layers on albite surfaces during dissolution under hydrothermal conditions. *Geochim. Cosmochim. Acta* **54**, 1267–1281.
- Hellmann, R., Penisson, J.-M., Hervig, R.L., Thomassin, J.-H., Abrioux, M.-F., 2003. An EFTEM/HRTEM high-resolution study of the near surface of labradorite feldspar altered at acid pH: evidence for interfacial dissolution-precipitation. *Phys. Chem. Min.* **30**, 192–197.
- Hellmann, R., Penisson, J.M., Hervig, R.L., Thomassin, J.H., Abrioux, M.F., 2004. Chemical alteration of feldspar: a comparative study using SIMS and HRTEM/EFTEM. In: Wanty, R.B., Seal, R.R. (Eds.), *Water-rock Interaction 11*, Saratoga Springs, New York, June 27–2 July 2004, A.A. Balkema, pp. 753–756.
- Hereford, A.G., Guthrie, G.D.J., Keating, E.H., Zhu, C., Zhu, L., 2005. Silicate reaction kinetics in the Pajarito Plateau, New Mexico. *Geological Society of America Abstr. with Programs* **37** (7), 381.
- Hochella, M.F., Banfield, J.F., 1995. Chemical weathering of silicates in nature: microscopic perspective with theoretical considerations. In: White, A.F., Brantley, S.L. (Eds.), *Chemical Weathering Rates of Silicate Minerals*, Vol. 31. Mineralogical Society of America.
- Hochella, M.F., Ponader, H.B., Turner, A.M., Harris, D.W., 1988. The complexity of mineral dissolution as viewed by high resolution scanning Auger microscopy: labradorite under hydrothermal conditions. *Geochim. Cosmochim. Acta* **52**, 385–394.
- Hodson, M.E., 2003. The influence of Fe-rich coatings on the dissolution of anorthite at pH 2.6. *Geochim. Cosmochim. Acta* **67** (18), 3355–3363.
- Holdren, G.R., Speyer, P.M., 1985. pH dependence changes in the rates and stoichiometry of dissolution of an alkali feldspar at room temperature. *Am. J. Sci.* **285**, 994–1026.
- Innskeep, W.P., Nater, E.A., Bloom, P.R., Vandervoort, D.S., Erich, M.S., 1991. Characterization of laboratory weathered labradorite surfaces using X-ray photoelectron spectroscopy and transmission electron microscopy. *Geochim. Cosmochim. Acta* **55**, 787–800.
- Lagache, M., 1965. Contribution à l'étude de l'altération des feldspaths, dans l'eau, entre 100 et 200 °C, sous diverses pressions de CO<sub>2</sub>, et application à la synthèse des minéraux argileux. *Bull. Soc. franc. Miner. Crist.* **88**, 223–253.
- Lagache, M., 1976. New data on the kinetics of the dissolution of alkali feldspars at 200°C in CO<sub>2</sub> charged water. *Geochim. Cosmochim. Acta* **40**, 157–161.
- Lagache, M., Wyart, J., Sabatier, G., 1961a. Dissolution des feldspaths alcalins dans l'eau pure ou chargée de CO<sub>2</sub> à 200 °C. *Acad. Sci. Paris, Comptes Rendus* **253**, 2019–2022.
- Lagache, M., Wyart, J., Sabatier, G., 1961b. Mécanisme de la dissolution des feldspaths alcalins dans l'eau pure ou chargée de CO<sub>2</sub> à 200 °C. *Acad. Sci. Paris, Comptes Rendus* **253**, 2296–2299.
- Lasaga, A.C., 1998. *Kinetic Theory in the Earth Sciences*. Princeton University Press, New York.
- Libarkin, J.C., Chase, C.G., 2003. Timing of Colorado Plateau uplift: Initial constraints from vesicular basalt-derived paleoelevations: comment. *Geology* **31** (2), 191–192.



- McGrail, B.P., Kumar, A., Day, D.E., 1984. Sodium diffusion and leaching of simulated nuclear waste glass. *J. Am. Ceramics Society* **67**, 463–467.
- Moore, D.M., Reynolds, J.R.C., 1997. *X-ray Diffraction and the Identification and Analysis of Clay Minerals*. Oxford University Press, Oxford, UK.
- Mucke, A., 1994. Part I. Postdiagenetic ferruginization of sedimentary rocks (sandstones, oolitic ironstones, kaolins and bauxites)—including a comparative study of the reddening of the red beds. In: Wolf, K.H., Chilingarian, G.V. (Eds.), *Diagenesis, Developments in Sedimentology*, vol. 4. Elsevier, New York, pp. 361–423.
- Muir, I., Bancroft, G.R., Nesbitt, H.W., 1990. A SIMS and XPS study of dissolving plagioclase. *Geochim. Cosmochim. Acta* **54**, 2247–2256.
- Murphy, W.M., Helgeson, H.C., 1987. Thermodynamics constraints and kinetic constraints on reaction rates among minerals and aqueous solutions III. Activated complexes and the pH-dependence of rates of feldspar, pyroxene, wollastonite and olivine hydrolysis. *Geochim. Cosmochim. Acta* **51**, 3137–3153.
- Nesbitt, H.W., Muir, I., 1988. SIMS depth profiles of weathered plagioclase and processes affecting dissolved Al and Si in some acidic soil solutions. *Nature* **334**, 336–338.
- Nesbitt, H.W., Skinner, W.M., 2001. Early development of Al, Ca, and Na compositional gradients in labradorite leached in pH 2 HCl solutions. *Geochim. Cosmochim. Acta* **65** (5), 715–727.
- Net, L., 2003. Diagenesis and reservoir quality of the Eolian Nugget/Navajo Sandstone (Early Jurassic), Utah and Wyoming. Master, University of Texas, Austin.
- Nugent, M.A., Brantley, S.L., Pantano, C.G., Maurice, P.A., 1998. The influence of natural mineral coatings on feldspar weathering. *Nature* **395** (6702), 588–591.
- Oelkers, E.H., 2001. General kinetic description of multioxide silicate mineral and glass dissolution. *Geochim. Cosmochim. Acta* **65** (21), 3703–3719.
- Paces, T., 1983. Rate constants of dissolution derived from the measurements of mass balance in hydrological catchments. *Geochim. Cosmochim. Acta* **37**, 1855–1863.
- Pederson, J.L., Mackley, R.D., Eddleman, J.L., 2002. Colorado plateau uplift and erosion evaluated using GIS. *Geotimes* **12** (8), 4–10.
- Penn, R.L., Zhu, C., Xu, H., Veblen, D.R., 2001. Iron oxide coatings on sand grains from the Atlantic coastal plain: HRTEM characterization. *Geology* **29** (9), 843–846.
- Peterson, F., 1988. Pennsylvania to Jurassic eolian transportation systems in the western United States. *Sediment. Geol.* **56**, 207–260.
- Petit, J.C., Dran, J.C., Della Mea, G., 1990. Energetic ion beam analysis in the earth sciences. *Nature* **344**, 621–626.
- Petit, J.C., Dran, J.C., Paccagnella, A., Della Mea, G., 1989. Structural dependence of crystalline silicate hydration during aqueous dissolution. *Earth Planet. Sci. Lett.* **93**, 292–298.
- Petrovic, R., 1976. Rate control in feldspar dissolution II. The protective effects of precipitates. *Geochim. Cosmochim. Acta* **40**, 1509–1521.
- Rahl, J.M., Reiners, P.W., Campbell, I.H., Nicolescu, S., Allen, C.M., 2003. Combined single-grain (U–Th)/He and U/Pb dating of detrital zircons from the Navajo sandstone, Utah. *Geology* **31** (9), 761–764.
- Sahagian, D., Proussevitch, A., Carlson, W., 2003. Timing of Colorado Plateau uplift: Initial constraints from vesicular basalt-derived paleoelevations: reply. *Geology* **31** (2), 192.
- Schott, J., Petit, J.C., 1987. New evidence for the mechanisms of dissolution of silicate minerals. In: Stumm, W. (Ed.), *Aquatic Surface Chemistry*. John Wiley, USA, pp. 293–318.
- Schweda, P., 1990. Kinetics and mechanisms of alkali feldspar dissolution at low temperatures. Ph.D. dissertation, Stockholm University.
- Smets, B.M.J., Tholen, M.G.W., 1985. The pH dependence of the aqueous corrosion of glass. *Phys. Chem. Glasses* **26**, 60–63.
- Swartz, C.H., Ulery, A.L., Gschwend, P.M., 1997. An AEM-TEM study of nanometer-scale mineral associations in an aquifer sand: implications for colloid mobilization. *Geochim. Cosmochim. Acta* **61** (4), 707–718.
- Velbel, M.A., 1985. Geochemical mass balances and weathering rates in forested watersheds of the southern Blue Ridge. *Am. J. Sci.* **285**, 904–930.
- Velbel, M.A., 1990. Influence of temperature and mineral surface characteristics on feldspar weathering rates in natural and artificial systems: a first approximation. *Water Resources Res.* **26**, 3049–3053.
- Whalley, W.B., Smith, B.J., McAlister, J.J., Edwards, A.J., 1987. Aeolian abrasion of quartz particles and the production of silt-size fragments: preliminary results. In: Frostick, L.E., Reid, I. (Eds.), *Geological Society Special Publications*, vol. 35. pp. 129–138.
- White, A.F., Brantley, S.L., 2003. The effect of time on the weathering of silicate minerals: why do weathering rates in the laboratory and field? *Chem. Geol.* **202**, 479–506.
- White, A.F., Bullen, T.D., Schulz, M.S., Blum, A.E., Huntington, T.G., Peters, N.E., 2001. Differential rates of feldspar weathering in granitic regoliths. *Geochim. Cosmochim. Acta* **65** (6), 847–869.
- Worden, R.H., Burley, S.D., 2003. Sandstone diagenesis: the evolution of sand to stone. In: Burley, S.D., Worden, R.H. (Eds.), *Sandstone Diagenesis—Recent and Ancient*, vol. 4. Blackwell, USA, pp. 3–47.
- Zhu, C., 2000. Estimate of recharge from radiocarbon dating of groundwater ages and numerical flow and transport modeling. *Water Resources Res.* **36** (9), 2607–2620.
- Zhu, C., 2005. In situ feldspar dissolution rates in an aquifer. *Geochim. Cosmochim. Acta* **69** (6), 1435–1453.
- Zhu, C., Blum, A., Veblen, D., 2004. Feldspar dissolution rates and clay precipitation in the Navajo aquifer at Black Mesa, Arizona, USA. *Proceedings of the Eleventh International Symposium on Water-Rock Interaction WRI-11*, 2, pp. 895–899.
- Zhu, C., Blum, A.E., 2005. In situ silicate dissolution and precipitation rates in sandy aquifers. *Geological Society of America Abstr. with Programs* **37** (7), 319.
- Zhu, C., Waddell, R.K., Star, I., Ostrander, M., 1998. The responses of groundwater in the Black Mesa basin, northeastern Arizona to paleoclimatic changes during late Pleistocene and Holocene. *Geology* **26**, 27–130.